2012 IEEE/RSJ International Conference on
Intelligent Robots and Systems
October 7-12, 2012. Vilamoura, Algarve, Portugal

On the role of load motion compensation in high-performance force control

Thiago Boaventura, Michele Focchi, Marco Frigerio,
Jonas Buchli, Claudio Semini, Gustavo A. Medrano-Cerda, Darwin G. Caldwell

Department of Advanced Robotics, Istituto Italiano di Tecnologia(IIT), via Morego, 30, 16163 Genova
{thiago.boaventura, michele.focchi, marco.frigerio, jonas.buchli, claudio.semini, gustavo.cerda, darwin.caldwell} @iit.it

***Abstract*— Robots are frequently modeled as rigid body systems, having torques as input to their dynamics. A high-performance low-level torque source allows us to control the robot/environment interaction and to straightforwardly take advantage of many model-based control techniques. In this paper, we define a general 1-DOF framework, using basic physical principles, to show that there exists an intrinsic velocity feedback in the generalized force dynamics, independently of the actuation technology. We illustrate this phenomena using three different systems: a generic spring-mass system, a hydraulic actuator, and an electric motor. This analogy helps to clarify important common aspects regarding torque/force control that can be useful when designing and controlling a robot. We demonstrate, using simulations and experimental data, that it is possible to compensate for the load motion influence and to increase the torque tracking capabilities.**

I. INTRODUCTION

Since the very early days of the development of articulated robots, torque control was of fundamental interest [1]. Torque control allows various forms of impedance control, control of contact forces, rigid body dynamics model-based control, virtual model control [2], operational space control [3], etc. Having these control capabilities is not only desirable but mandatory for robust performance of robots in unstructured and partially unknown environments [4]. Torque control also allows the development of versatile and robust articulated robots that can be used in a wide variety of applications, e.g. disaster recovery, construction, service robots, etc [5].

Research on robot torque/force control began in the 1950s with remote manipulators, but stability issues emerged immediately [1]. For position-controlled systems, stiff mechanical interfaces between the actuator and its load raise the system bandwidth without compromising stability [6]. For force-controlled systems, however, this stiff transmission is the main reason for stability problems. A way to overcome such issues has been found in reducing the transmission stiffness, and consequently the overall system bandwidth. Initially, it was done by using flexible sensors, and more recently by introducing springs in series with the actuator [7].

However, softness isn't everything. Advanced control approaches, such as model-based control, can be successfully applied in the low-level force control to reach a good tracking performance without having to give up on the bandwidth. Since the force is always transmitted from the actuator to the load through a transmission with finite stiffness (e.g. gearbox, hydraulic oil, spring), there exist an intrinsic load velocity feedback in the force dynamics, which does not depend on the actuator. An important model-based control consists in compensating for this physical load motion feedback.

The load motion compensation was initially discussed for hydraulic actuators in [8], where it is shown that closed-loop control with force feedback is ineffective without velocity feedforward, or full state feedback. The influence of the load motion is shown for a hydraulic actuator in [9]. The authors called this concept *natural velocity feedback*. In [10], a solution to negate the natural velocity feedback of the actuator was proposed.

Previous works addressed the compensation of the load motion for electrical drives as well. Hori et al [11] implemented disturbance observers to compensate for the effect of the load torque by feeding back the motor velocity signal. Dhaouadi et al [12] designed a speed controller based on a torque observer to increase the phase margin at the resonant frequency and to reduce the limit cycles resulting from the gear backlash. Kaneko et al [13] attained similar results designing an acceleration controller and using positive feedbacks from torque and load position. This suppressed the effects of both load torque and motor friction, setting a single inertia behavior to the system.

Even if the load motion compensation has been investigated in previous works, a general framework for this problem is currently missing in the literature. In this work, we summarize the generalized force control problem, for one degree of freedom (DOF), into a common framework with only three elements: a velocity source, a transmission, and a load. We draw a parallel between a generic mechanical case, and the two different actuators employed in the quadruped robot HyQ [14]: electric and hydraulic. This analogy emphasizes that the feedback of the load velocity exists independently on the actuation system and also helps clarifying important robot design aspects that can be useful when building a robot. We identify crucial concepts in force control which can help, for instance, robot designers choose the actuation type and the transmission stiffness that best fit the robot application requirements. Another contribution of this work is to show simulation and experimental results that verify the significant improvement in the torque/force closed-loop control bandwidth due to the load motion compensation.

The paper is structured as follows: in Sec. II, we show the intrinsic load motion feedback in the force dynamics for a generic mechanical case, and then for hydraulic and electric actuators. Sec. III presents how to compensate for this load velocity influence and Sec. IV describes the simulation and experimental results for the proposed compensation. Relevant force control issues are discussed in Sec. V before finishing the paper with conclusions and future work in Sec. VI.

978-1-4673-1735-1/12/S31.00 ©2012 IEEE

II. Load Motion in the Force Dynamics

Force is always controlled over a transmission element that is deformable or compressible. The force is transmitted from the actuator to the load through this compliant transmission element, where the force is normally measured. The force sensor is usually much stiffer than the transmission, and within this paper we will not consider its compliance. In Fig. 1, we show a basic mechanical system composed of an ideal velocity source *vs*, a transmission with stiffness K_t, a generic *load*, and the force F transmitted to the load.

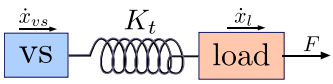

Fig. 1. Generic spring-mass system representing a velocity source, that drives a load through a compliant transmission.

Since springs are impedances, they have velocity as input to their dynamics and force as output. On the other hand, masses are admittances and have forces as input and velocity as output to their dynamics [15]. In Fig. 1, the velocity source *vs* is a mass, accelerated by an external actuator, and has an instantaneous velocity $\dot{x}_{vs}$, which is transmitted to the transmission spring. The spring output force F acts on the load mass, which is accelerated and has an instantaneous velocity $\dot{x}_l$. The load force dynamics $\dot{F}$ can be written as:

$$\dot{F} = K_t \left(\dot{x}_{vs} - \dot{x}_l \right) \tag{1}$$

The presence of $\dot{x}_l$ in (1) underlines that the dynamics of the force that is transmitted to the load depends also on the load itself, and not only on the actuator. The actuator dynamics defines how quickly the velocity $\dot{x}_{vs}$ can be changed. On the other hand, the load dynamics determines how fast the load velocity $\dot{x}_l$ changes given an input force.

This interaction between force and load dynamics is intrinsic to the physics, no matter the actuation and load characteristics, and it can be mathematically seen as a *load velocity feedback*. Based on the block diagram of Fig. 2, given that M_l is the mass and B_l is the damping of the load, we can calculate the following transfer function:

$$\frac{F(s)}{\dot{x}_{vs}(s)} = \frac{K_t \left(M_l s + B_l \right)}{s \left(M_l s + B_l \right) + K_t} \tag{2}$$

Looking at Fig. 2, we can notice that the pole of the load dynamics appears also as a zero of the force transfer function in (2). This result occurs regardless of how fast the actuation dynamics is [9]. Thus, in a force closed-loop, both the controller gain and the performance of the system are limited by the frequency of this zero.

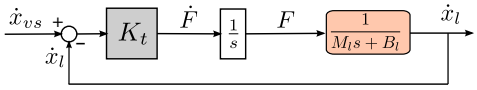

Fig. 2. Block diagram for a generic velocity source, acting on a load through a transmission stiffness. The load velocity $\dot{x}_l$ is clearly being fed back into the load force dynamics.

Next, we will go into the details of the two different actuation systems present on the HyQ platform: electric and hydraulic. We will show that their models fit well into the generic mechanical case we considered in this section.

A. Hydraulic actuation

In hydraulics, the velocity source is the pump and valve together. The pump pressurizes the fluid and the valve controls the fluid flow that is going into the hydraulic cylinder. An accumulator is usually placed upstream of the valve to compensate for the pump dynamics and eventual pressure drops so that we can consider the supply line as a perfect pressure source. Therefore, the velocity source dynamics is determined only by the valve and flow dynamics. The transmission is characterized by the fluid, and the transmission stiffness by the fluid compressibility and volume.

Since the cylinder rod is usually rigidly attached to the load, it can be considered part of it. In this work, we consider the cylinder friction as part of the load dynamics. Thus, for an asymmetric hydraulic cylinder, and neglecting cylinder leakage, the hydraulic force dynamics $\dot{F}_h$ can be calculated by doing a balance between the forces created in the cylinder chambers a and b [16]:

$$\dot{F}_h = \frac{A_p \beta}{V_a} \left(Q_a - A_p \dot{x}_l \right) - \frac{\alpha A_p \beta}{V_b} \left(-Q_b + \alpha A_p \dot{x}_l \right) \tag{3}$$

where A_p is the piston area; α is the piston/annulus-area ratio (i.e., $A_a = A_p$ and $A_b = \alpha A_p$); β is the oil's bulk modulus; V_a and V_b are the variable chamber volumes, which are a function of the cylinder position x_l, and include the pipe volumes; Q_a is the valve flow that is going into the chamber a, and Q_b the flow going out of chamber b.

As we can notice, (3) is composed of two different forces, each one in the same generic form described in (1), that is: a *controllable input velocity*, represented by a flow; the *link velocity*, in this case multiplied by a gain that is equal to the respective chamber area; and a *transmission stiffness*, which depends on the bulk modulus and on the chamber area and volume.

To obtain a block diagram similar to the one shown in Fig. 2, we can model the two different hydraulic transmission stiffnesses, created by the two cylinder chambers, as parallel springs [17]. Then, we can define a resultant hydraulic stiffness K_{th} and rewrite the hydraulic force dynamics as:

$$\dot{F}_h = K_{th} \left(Q_e - A_e \dot{x}_l \right) \tag{4}$$

where Q_e is an equivalent flow, and A_e an equivalent area. K_{th}, Q_e, and A_e are defined in the Appendix.

The hydraulic flow that passes across the valve depends on the valve flow gain, on the valve spool opening, and also on the square root of the pressure difference between the valve ports. To fully understand the influence of the load motion velocity in hydraulics, we will linearize the nonlinear pressure-flow characteristics present in Q_e. Thus, the following transfer function can be written [18]:

$$\frac{F_h(s)}{V_v(s)} = \frac{\frac{K_{qe}}{K_{pe}} \left(M_l s + B_l \right)}{\left(M_l s + B_l \right) \left(-1 + \frac{1}{K_{th} K_{pe}} s \right) + \frac{A_e}{K_{pe}}} \tag{5}$$

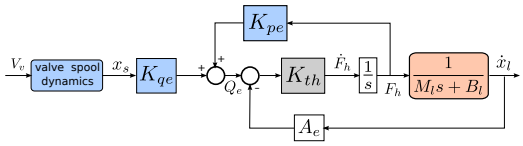

Fig. 3. Block diagram for a hydraulic actuator. The load velocity is multiplied by the equivalent area A_e and is transformed in a flow. This flow is then fed back into the force dynamics.

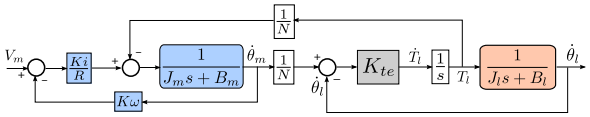

Fig. 4. Block diagram for an electric motor: once again, the load angular velocity feedback is clearly present in the dynamics.

where K_{qe} and K_{pe} are equivalent weighted versions of the flow and flow-pressure gains, respectively [16] (see their algebraic definition in the Appendix). V_v is the voltage applied to the valve. The equivalent hydraulic block diagram for the linearized system is depicted in Fig. 3.

In (5), we are neglecting the valve spool dynamics shown in Fig. 3. For the valves used in HyQ [19], the dynamics for the spool displacement x_s can be approximated by a second order system with natural frequency around $\omega_v = 1600\ rad/s$ and damping $D_v = 0.5$, which is several times faster than the pressure and load motion dynamics.

B. Electric actuation

An electric motor has its rotor as velocity source for the transmission, which in most of the cases in robotics consists of a gear box. The gear box introduces an elasticity between the rotor and the load. This elasticity defines the rotational transmission stiffness K_{te} for the electric actuation. HyQ uses a harmonic drive with ratio 1:100 and stiffness $K_{te} = 2.7 \cdot 10^4\ Nm/rad$ [20]. The dynamics of the torque T_l transmitted to the load is the rotational version of the linear dynamics shown in (1), that is:

$$\dot{T}_l = K_{te}\left(\frac{\dot{\theta}_m}{N} - \dot{\theta}_l\right) \tag{6}$$

where $\dot{\theta}_m$ and $\dot{\theta}_l$ are the angular velocities of the rotor and load, respectively, and N is the gear ratio.

The motor dynamics can be modeled as a second order system, with inertia J_m and damping coefficient B_m, which includes both rotor and gear box viscous frictions. Considering a load with inertia J_l and damping B_l, the following transfer function from the input voltage to the load torque can be obtained (see the Appendix for model equations):

$$\frac{T_l(s)}{V_m(s)} = \frac{K_i K_{te}(J_l s + B_l)N}{\Psi N^2(R(J_m s + B_m) + K_i K_\omega) + R K_{te}(J_l s + B_l)} \tag{7}$$

where $\Psi = \left(J_l s^2 + B_l s + K_{te}\right)$, V_m is the input voltage, K_i and K_ω are the torque-current and back-emf motor constants, respectively, and R is the motor coil resistance. The electrical voltage-to-current dynamics is neglected. As for the previous cases, the torque transfer function has a zero due to the load dynamics. All the poles (one real and two complex) depend on both load and motor parameters. The corresponding block diagram is shown in Fig. 4.

III. Load Motion Compensation

As described in the previous sections, the dynamics of the force/torque that is transmitted from the actuator to the load depends not only on the actuator dynamics but also on the load dynamics. However, if we want to control this load force, it is desirable that its dynamics only depends on the variable we can directly actuate, which is, for the generic mechanical case, the velocity $\dot{x}_{vs}$.

An intuitive way for compensating this load motion influence is to measure the load velocity $\dot{x}_l$ and to *continuously* apply, with our ideal velocity source, an extra velocity $\dot{x}_{ex} = \dot{x}_l$. In this case, the load force dynamics is given by:

$$\dot{F} = K_t\left[(\dot{x}_{vs} + \dot{x}_{ex}) - \dot{x}_l\right] = K_t \dot{x}_{vs} \tag{8}$$

Taking (8) into account , we can write the transfer function for the velocity-compensated system as:

$$\frac{F(s)}{\dot{x}_{vs}(s)} = \frac{K_t}{s} \tag{9}$$

The mathematical effect of the load velocity compensation is to algebraically eliminate the term K_t from the denominator of (2). This is equivalent to open the natural loop created by the load velocity feedback. By eliminating this term, a perfect zero/pole cancellation becomes possible and the same velocity-compensated dynamics (9) is obtained. To cancel out the influence of the zero on the force dynamics is the main consequence of the load motion compensation. With this zero/pole cancellation, we are then able to increase the gains without making the system unstable, taking the dominant closed-loop pole to higher frequencies.

Considering a more realistic scenario, where we do not have an ideal velocity source, this extra velocity $\dot{x}_{ex}$ has to be created by the actuator, which has its own dynamics. If this actuator dynamics influences significantly the force dynamics, we also need to take it into account when compensating for the load motion.

In the next sections, we show how to perform this load motion compensation for both actuation types of HyQ. We demonstrate that the zero/pole cancellation happens independently of the actuation system.

A. Hydraulic Actuation

Considering a hydraulic actuator, the extra velocity $\dot{x}_{ex}$, represents an extra flow Q_{ex} that has to be supplied by the valve. This extra flow must be $Q_{ex} = A_e \dot{x}_l$ in order to perfectly compensate for the load motion influence.

To supply this extra flow Q_{ex}, we have to consider the flow dynamics, but as mentioned before we will neglect the valve spool dynamics. We assume that a valve input voltage V_v is instantaneously converted into valve spool opening x_s. Thus, feeding back the load velocity $\dot{x}_l$, the valve input $V_{v_{vc}}$ that compensates for the velocity feedback is:

$$V_{v_{vc}} = \frac{A_e \dot{x}_l}{K_{qe}} \tag{10}$$

In terms of block diagram, to supply this extra flow Q_{ex} is equivalent to opening the velocity loop, or making $A_e = 0$ in Fig. 3. By looking at (5), we can notice that, by algebraically eliminating the term A_e/K_{pe}, we have the same zero/pole cancellation as discussed before.

B. Electric Actuation

For an electric motor, the velocity compensation is not as intuitive as for the hydraulic case. By inserting the motor dynamics (first equation of (17) in the Appendix) into (6), we can work out the expression of the motor voltage $V_{m_{vc}}$ that compensates for load motion:

$$V_{m_{vc}} = \frac{NR}{K_i}\left(J_m s + \frac{K_i K_\omega}{R} + B_m\right)\dot{\theta}_l \qquad (11)$$

In terms of transfer function, the effect of the compensation is the algebraic elimination of the term K_{te} in the variable we abbreviated as Ψ. This allows to cancel the pole $(J_l s + B_l)$ with its respective zero. The compensated system becomes a second order system and the poles depend only on motor parameters B_m, J_m, K_i, K_w and on transmission stiffness K_{te}, and no longer on load dynamics (B_l and J_l).

IV. Results

As previously discussed, the main consequence of the load motion compensation into the force dynamics is a zero/pole cancellation. In this section, we demonstrate, through simulations and experiments on both actuation systems of the HyQ robot, a significant improvement on the force/torque tracking capabilities by compensating for the load velocity.

A. Simulation Results

In this section we present the results we obtained simulating the models we showed in the previous sections. We compare, for both actuators, the force tracking performance with and without the proposed velocity compensation.

A PID controller has been tuned differently for the compensated and non-compensated system. In all cases, the gains were chosen to obtain the fastest non-oscillatory closed-loop response possible (margin phase of at least 60 deg).

In Fig. 5, we used parameters based on the hydraulic system of HyQ to simulate the linear force dynamics for a hydraulic cylinder driving a load with mass $M_l = 50\ kg$ and damping $B_l = 700\ Ns/m$. We can see that the velocity-compensated system has a much smaller settling time than

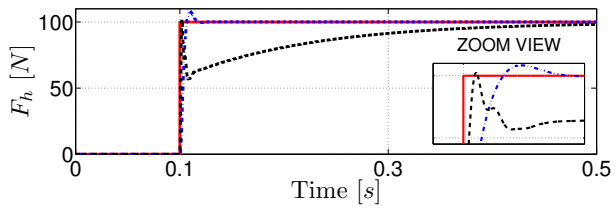

Fig. 5. Force step response for a hydraulic cylinder. The solid red line shows the force reference, the dashed black the non-compensated response, and the dot-dashed blue line the response when the load motion is compensated for. The zoom view, around 0.1 s, clearly shows the force drop due to the load motion influence.

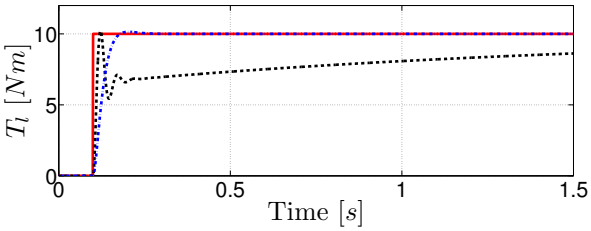

Fig. 6. Torque step response for a electric motor. The solid red line shows the torque reference, the dashed black the non-compensated response, and the dot-dashed blue line the load velocity-compensated response.

the non-compensated one. Furthermore, the influence of the load motion is clearly seen in the non-compensated response. It raises as quickly as the compensated one, but after a short period the force magnitude drops drastically. This drop happens exactly when the load starts to move, "uncompressing" the transmission spring, reducing the oil pressure inside the chamber, and consequently the force.

For the electric motor, we applied a torque step to a load with inertia $J_l = 1\ Kgm^2$ and damping $B_l = 1\ Nms/rad$. In Fig. 6, we can see that the behavior of both responses are very similar to the hydraulic case. It demonstrates that, independently of the actuator, to compensate for the load motion increases significantly the force/torque bandwidth and tracking capabilities.

B. Experimental

HyQ is a quadruped robot that weighs about 70 kg, is 1 m long, and 1 m tall with fully stretched legs [14]. HyQ's legs have 3 degrees of freedom (DOF) each, being the hip and knee flexion/extension (HFE and KFE, respectively) hydraulically actuated, and the hip abduction/adduction (HAA), electrically actuated. The maximum joint torque for both actuators is about 140 Nm. The hydraulic force is measured by a load cell placed at the end of the cylinder rod and the torque created by the electric motor by a custom torque sensor based on strain gages.

To demonstrate the influence of the velocity compensation on a real system, we implemented a torque step of 10 Nm, which is applied at the same time for both the HFE and HAA joints. We fixed a 5 kg weight to the leg end-effector to create an artificial load and permit a reasonable torque step magnitude. We compare in Fig. 7 the system response with and without velocity compensation for both actuators.

The hydraulic response followed the simulation results presented in the previous section. We can notice, for the non-compensated case, that the force has a longer settling time because of a force drop due to the load motion. For the electric motor, differently from the simulation, oscillations at 12 Hz are present in the compensated-response. This is a side effect of velocity compensation, which introduces a resonance peak at that frequency. It does not show up in the simulation results because of a modeling simplification, which does not consider the leg flexibility. The effect of this high torque frequency is significantly filtered by leg inertia and does not affect the leg motion.

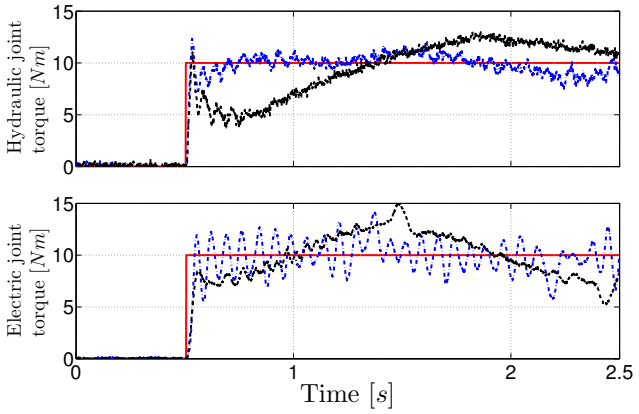

Fig. 7. Response to a step torque reference for the hydraulic hip joint HFE (upper plot) and the electric hip joint HAA (lower plot); in dashed black the non-compensated response, and in dot-dashed blue the compensated one.

V. Discussion

If no velocity compensation is used, the force closed-loop performance is limited by the zero due to the load dynamics. Considering a PI controller, this load zero attracts the pole of the controller integrator and prevents it from going to higher frequencies. For a non-oscillatory response, this low-frequency pole will be the dominant one and it will limit system velocity in closed-loop. As we can see in (2), the higher the friction B_l, the higher the frequency of the zero, and consequently the faster the force dynamics can be. In hydraulics, the piston is part of the load and it has a significant friction due to its tight sealing with the cylinder body. On the other hand, electric motors use bearings and the friction is much smaller. Therefore, even without velocity compensation, hydraulic actuators tend to have better force closed-loop performance than electric motors.

As we demonstrated in Sec. III, the velocity compensation cancels the zero presented in the force dynamics. This cancellation allows us to increase the controller gains and put the dominant pole at high frequencies without making the system unstable. However, the velocity compensation is a model-based compensation and is therefore susceptible to parameter uncertainties. Then, a perfect zero/pole cancellation is as challenging as creating a perfect model. In practice, the velocity will be either under or over compensated.

In the zero-pole map of Fig. 8, we show the dominant open-loop poles for different levels of under and over compensations. An under compensation places both dominant open-loop poles at the left side of the zero, and an over compensation places one at its left and one at its right. We can demonstrate that, by closing a loop with a PI controller, the dominant closed-loop pole of the under-compensated system is still limited by the frequency of the zero. For the over-compensated case, the dominant pole can go beyond the zero frequency, increasing the system bandwidth. However, a slight over-compensation can make the system unstable for certain controller gains, reducing the robustness.

Another possible practical issue for the electric actuation is that the velocity compensation also includes the acceleration,

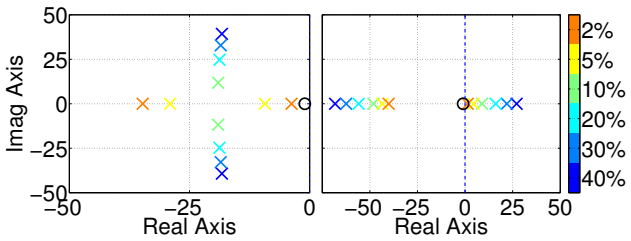

Fig. 8. Root locus of the open-loop poles for the electric actuation: On the left plot we show the under-compensation case, and on the right side we show the over-compensation case. The color bar illustrates different percentages of under/over compensations.

which is usually quite jerky due to the double numerical differentiation. However, simulation and empirical results showed that the influence of the term $J_m s\dot{\theta}_l$ in (11) is not significant in the range of frequencies of interest and that it can be neglected. Furthermore, aggressive digital filtering can introduce significant time delays, making the system unstable.

Force control is always done through a compliant transmission element. In series elastic actuators (SEA), the spring works also as a low-pass filter, lowering the transmission stiffness. This reduced overall stiffness matches the available actuator bandwidth, reducing the difficulty of the torque control issue. However, in this approach the achievable load force bandwidth is limited by the stiffness of the spring: the softer the spring, the slower the load force dynamics will be. The most appropriate spring stiffness is certainly a very difficult parameter to select and this choice can seriously limit the robot's dynamic performance and versatility.

The very small fluid compressibility makes the hydraulic transmission intrinsically stiff. Some design aspects, such as the flexibility of the pipes, can reduce this high hydraulic stiffness. All these aspects define the *bulk modulus* of the hydraulic system. However, as we can see in the definition of K_{th} in (12), the hydraulic transmission stiffness depends also on the chamber volumes. Differently from real springs, that transform a certain displacement in force, the hydraulic stiffness transforms a certain piston displacement into pressure. To obtain a stiffness in N/m, which has a more intuitive meaning for us, we must multiply the stiffness K_{th} by the equivalent area A_e. The result of this multiplication, considering HyQ's parameters, is plotted in Fig. 9.

Since the stiffness is higher at the minimum and maximum positions, the system will be more reactive at these positions,

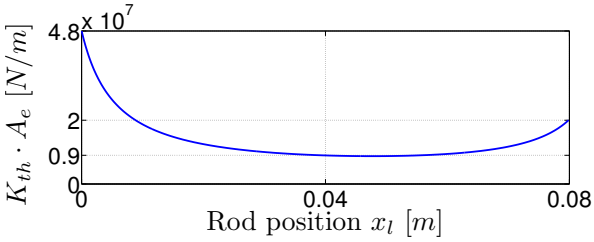

Fig. 9. Hydraulic stiffness of the assymetric cylinder of HyQ: it depends on the fluid properties, on the cylinder areas, on the pipe length, and on the cylinder rod position.

and the force control more challenging. At these extreme positions, the stiffness magnitude depends directly on the pipe line volume that connects the valve to the cylinder chamber. When the pipe volume tends to zero, the stiffness tends to infinity. Thus, the pipe volume plays an important role in the robot design and it must be taken into account when matching the transmission stiffness to the actuator bandwidth, which is defined by the valve dynamics. HyQ uses valves with a bandwidth of $250\ Hz$. These fast valves are able to cope with the high stiffness plotted in Fig. 9, which has a minimum value of $0.9 \cdot 10^7\ N/m$.

VI. Conclusions and future work

Independently of the actuator and load characteristics, there will always exist an intrinsic interaction between the actuator and its load, that limits the torque (or generalized force) closed-loop performance. This interaction happens as a velocity feedback in the force dynamics.

We have designed model-based control laws that compensate for this velocity feedback in two different actuation systems: hydraulic and electric. We have shown simulations and experiments that verify that this compensation increases notably the force tracking capabilities.

Future work includes the definition of a simple set of rules to find the required actuator bandwidth to perform high-performance force control over a known transmission stiffness. The passivity with velocity compensation will also be investigated when closing an external impedance loop and for a system with more DOFs. A more refined model for the electric actuation, which captures the resonant effect of the velocity compensation by considering the sensor inertia and the load flexibility, is work in progress.

The work we presented in this paper aimed to highlight the importance of torque control on robotics and to give a valuable tool to improve its tracking performance. The closer we are to a perfect torque source, the faster we can move towards truly versatile robots.

Appendix

The hydraulic stiffness K_{th} can be defined by summing the two stiffnesses in (3):

$$K_{th} = A_p \beta \left(\frac{1}{V_a} + \frac{\alpha}{V_b} \right) \quad \left[\frac{Pa}{m} \right] \tag{12}$$

Then, through basic algebraic manipulation, it is possible to find an equivalent flow and area, which are defined as:

$$Q_e = \frac{V_b Q_a + \alpha V_a Q_b}{V_b + \alpha V a} \quad \left[\frac{m^3}{s} \right] \tag{13}$$

$$A_e = A_p \left(\frac{V_b + \alpha^2 V_a}{V_b + \alpha V_a} \right) \quad \left[m^2 \right] \tag{14}$$

The linearized flow dynamics can be described using the flow gains K_{qa} and K_{qb}, and the flow-pressure gains K_{pa} and K_{pb} [16]. To match the equivalent force dynamics proposed by (4), these gains have to be redefined. The equivalent flow gain K_{qe} and the equivalent flow-pressure gain K_{pe} can be defines as:

$$K_{qe} = \frac{V_b K_{qa} + \alpha V_a K_{qb}}{V_b + \alpha V_a} \quad \left[\frac{m^3}{sV} \right] \tag{15}$$

$$K_{pe} = \frac{1}{A_p \left(1 + \alpha^3\right)} \left(\frac{V_b K_{pa} - \alpha^3 V_a K_{pb}}{V_b + \alpha V_a} \right) \quad \left[\frac{m}{sPa} \right] \tag{16}$$

The equations that describe the load and electrical motor dynamics are the following [13]:

$$\begin{aligned} & J_m \ddot{\theta}_m + B_m \dot{\theta}_m + \tfrac{K_{te}}{N} (\tfrac{\theta_m}{N} - \theta_l) = K_i I \\ & J_l \ddot{\theta}_l + B_l \dot{\theta}_l - K_{te} (\theta_m / N - \theta_l) = 0 \\ & I = \tfrac{V - K_w \dot{\theta}_m}{R} \\ & T_l = K_{te} \left(\tfrac{\theta_m}{N} - \theta_l \right) \end{aligned} \tag{17}$$

where I is the motor current. The electrical dynamics is neglected. Therefore, the current is obtained by an algebraic equation.

Acknowledgments

This research has been funded by the Fondazione Istituto Italiano di Tecnologia.

References

[1] D. E. Whitney, "Historical perspective and state of the art in robot force control," in *Robotics and Automation. Proceedings. 1985 IEEE International Conference on*, vol. 2, mar 1985, pp. 262 – 268.

[2] J. Pratt, C. Chew, A. Torres, P. Dilworth, and G. Pratt, "Virtual model control: An intuitive approach for bipedal locomotion," *Int Journal of Robotics Research*, vol. 20, no. 2, pp. 129–143, 2001.

[3] O. Khatib, "A unified approach for motion and force control of robot manipulators: The operational space formulation," *Robotics and Automation, IEEE Journal of*, vol. 3, no. 1, pp. 43–53, 1987.

[4] J. Buchli, M. Kalakrishnan, M. Mistry, P. Pastor, and S. Schaal, "Compliant quadruped locomotion over rough terrain," in *Proceedings of IEEE/RSJ International Conference on Intelligent Robots and Systems (IROS)*, 2009, pp. 814–820.

[5] T. Boaventura, C. Semini, J. Buchli, M. Frigerio, M. Focchi, and D. G. Caldwell, "Dynamic torque control of a hydraulic quadruped robot," in *IEEE ICRA*, 2012, pp. 1889–1894.

[6] R. H. J. Cannon and E. Schmitz, "Initial experiments on the end-point control of a flexible one-link robot," *Robotics Research, International Journal of*, vol. 3 No. 3, pp. 62–75, 1984.

[7] G. Pratt and M. Williamson, "Series elastic actuators," in *IEEE/RSJ IROS*, vol. 1, 1995, pp. 399 –406 vol.1.

[8] F. Conrad and C. Jensen, "Design of hydraulic force control systems with state estimate feedback," in *IFAC 10th Triennial Congress*, Munich, Germany, 1987, pp. 307–31.

[9] S. Dyke, B. Spencer Jr., P. Quast, and M. Sain, "Role of control-structure interaction in protective system design," *Journal of Engineering Mechanics, ASCE*, vol. 121 No.2, pp. 322–38, 1995.

[10] J. Dimig, C. Shield, C. French, F. Bailey, and A. Clark, "Effective force testing: A method of seismic simulation for structural testing," *J. Structural Engineering*, vol. 125, no. 9, pp. 1028–1037, 1999.

[11] Y. Hori, H. Iseki, and K. Sugiura, "Basic consideration of vibration suppression and disturbance rejection control of multi-inertia system using sflac," *IEEE Trans. Ind. Appl.*, vol. 30, no. 4, pp. 889–896, 1994.

[12] R. Dhaouadi, K. Kubo, and M. Tobise, "Analysis and compensation of speed drive systems with torsional loads," in *Proc. Conf Power Conversion Conf., Yokohama. Record of the*, 1993, pp. 271–277.

[13] K. Kaneko, N. Suzuki, K. Ohnishi, and K. Tanie, "High stiffness torque control for a geared dc motor based on acceleration controller," in *Proc. IECON '91. Conf. Int Industrial Electronics, Control and Instrumentation*, 1991, pp. 849–854.

[14] C. Semini, N. G. Tsagarakis, E. Guglielmino, M. Focchi, F. Cannella, and D. G. Caldwell, "Design of HyQ - a hydraulically and electrically actuated quadruped robot," *IMechE Part I: J. of Systems and Control Engineering*, vol. 225, no. 6, pp. 831–849, 2011.

[15] N. Hogan, "Impedance control: An approach to manipulation: Part I – Theory," *ASME, Transactions, Journal of Dynamic Systems, Measurement, and Control*, vol. 107, pp. 1–7, 1985.

[16] H. E. Merritt, *Hydraulic control systems*. Wiley-Interscience, 1967.

[17] S. Skinner and R. Long, *Closed Loop Electrohydraulic Systems Manual*, 2nd ed., Vickers, Rochester Hills, MI, 1998.

[18] M. Jelali and A. Kroll, *Hydraulic Servo-systems. Modelling, Identification and Control*. Springer, 2003.

[19] MOOG Inc., *Data Sheet of E024 Series Microvalve*, 2003.

[20] M. Focchi, T. Boaventura, C. Semini, M. Frigerio, J. Buchli, and D. G. Caldwell, "Torque-control based compliant actuation of a quadruped robot," in *Proc. of the 12th IEEE Int. Workshop on Advanced Motion Control (AMC)*, 2012.